On the key kinetic interactions between NO_X and unsaturated hydrocarbons: H-atom abstraction from C_3-C_7 alkynes, dienes and triene by NO_2

Zhengyan Guo[a,d,^], Hongqing Wu[b,^], Ruoyue Tang[b,^], Xinrui Ren[b], Ting Zhang[b], Mingrui Wang[b], Guojie Liang[b], Hengjie Guo[a], Song Cheng[b,c,*]

[a] *School of Power and Energy, Northwestern Polytechnical University, Xi'an 710129, China*
[b] *Department of Mechanical Engineering, The Hong Kong Polytechnic University, Kowloon, Hong Kong SAR 999077, China*
[c] *Research Institute for Smart Energy, The Hong Kong Polytechnic University, Kowloon, Hong Kong SAR 999077, China*
[d] *AECC Hunan Aviation Powerplant Research Institute, Zhuzhou 412002, China*

^ Authors contribute equally to this paper.

* Corresponding authors: Song Cheng

Phone: +852 2766 6668

Email: songryan.cheng@polyu.edu.hk

Abstract:

An adequate understanding of NO_x interacting chemistry is a prerequisite for a smoother transition to carbon-lean and carbon-free fuels such as ammonia and hydrogen. In this regard, this study presents a comprehensive study on the H-atom abstraction by NO_2 from C_3-C_7 alkynes, dienes and triene forming 3 HNO_2 isomers (i.e., TRANS_HONO, HNO_2, and CIS_HONO), encompassing 8 hydrocarbons and 24 reactions. Through a combination of high-level quantum chemistry computation, electronic structures, single point energies, C-H bond dissociation energies and 1-D hindered rotor potentials of the reactants, transition states, complexes and products involved in each reaction are determined at DLPNO-CCSD(T)/cc-pVDZ//M06–2X/6−311++g(d,p), from which potential energy surfaces and energy barriers for each reaction are determined. Following this, the rate coefficients for all studied reactions, over a temperature range from 298 to 2000 K, are computed based on transition state theory using the Master Equation System Solver program with considering unsymmetric tunneling corrections. Comprehensive analysis of branching ratios elucidates the diversity and similarities between different species, different HNO_2 isomers, and different abstraction sites. Incorporating the calculated rate parameters into a recent chemistry model reveals the significant influences of this type of reaction on model performance, where the updated model is consistently more reactive for all the alkynes, dienes and triene studied in predicting autoignition characteristics. Sensitivity and flux analyses are further conducted, through which the importance of H-atom abstractions by NO_2 is highlighted. With the updated rate parameters, the branching ratios in fuel consumption clearly shifts towards H-atom abstractions by NO_2 while away from H-atom abstractions by $\dot{O}H$. The obtained results emphasize the need for adequately representing these kinetics in new alkyne, diene and triene chemistry models to be developed by using the rate parameters determined in this study, and call for future efforts to experimentally investigate NO_2 blending effects on alkynes, dienes and triene.

Keywords: *H-atom abstraction reaction by NO_2; high-level ab initio calculations; NO_x interaction chemistry; rate rules; C_3-C_7 alkynes, dienes and triene*.

1. Introduction

The need for sufficient understanding of NO_x/hydrocarbon interactions has been more imminent than ever. On one hand, the recently growing interests in using ammonia as carbon-free alternative fuel for fossil-derived conventional fuels have advocated fuel-blending combustion as a means to address the poor combustion performance and high NO_x emissions of pure ammonia. Under this strategy, ammonia is typically bended with a more reactive hydrocarbon (e.g., n-heptane [1]), where the NO_x and NH_x species produced from ammonia chemistry can alter substantially the chemistry of the companion fuel. On the other hand, from the perspective of advanced engine operation, exhaust gas recirculation (EGR) has a long history in application to advanced internal combustion engines, enabling better and wider control of combustion phasing/heat release rates (HRRs) in homogeneous charge compression ignition engines [2] and knock in spark-ignition engines [3]. The use of EGR introduces both physical and chemical effects on engine combustion performance, among which the chemical influences of minor EGR species such as NO_x have been found to be significant [4] even at small in-cylinder concentrations (e.g., 10 – 250 ppm).

As such, in recent decades, extensive fundamental studies have been carried out for investigating the interactions between NO_x and typical hydrocarbons [4-9]. Both inhibiting and promoting effects of NO_x on fuel reactivity have been reported, highlighting the complicated NO_x/hydrocarbon interacting chemistries. While some understandings of the underlying kinetics have been gained through these studies, the existing studies still fall short in the following: (a) past studies mainly focused on NO with NO_2 largely overlooked; and (b) there is a severe lack of studies on unsaturated hydrocarbons, with most of the existing studies focusing on alkanes and aromatics. Menon et al. [10] examined the influence of NO_2 on the formation of soot precursors during the pyrolysis of ethylene in a flow reactor and reported significant impact of NO_2 on ethylene consumption and soot precursor formation. Deng et al.

[11,12] investigated high-pressure ignition characteristics of NO_2/C_2H_4 mixtures and NO_2/C_3H_6 mixtures in a shock tube. The experiments illustrated a significant decrease in the ignition delay time of ethylene and propylene with the presence of NO_2. Yuan et al. [13] conducted experimental and modeling analysis to explore the interaction kinetics between NO_2 and propylene in a laminar flow reactor. They found that the direct interactions between NO_2 and the fuel molecules and their primary derivatives are the major causes for the changed reactivity. Very recently, Cheng et al. [14] characterized the interactions between NO_x and ethylene/propylene/isobutylene in a rapid compression machine, and revealed the strong influences of these interactions on the autoignition reactivity of gasoline fuels. Through limited, these studies have consistently revealed a major type of interaction reactions directly involving NO_2, namely $RH+NO_2 = \dot{R}+HNO_2/HONO$, that greatly promotes reactivity.

There have been a few experimental and theoretical studies to determine the rate coefficients of $RH+NO_2 = \dot{R}+HNO_2/HONO$. Chai et al. [15] calculated the rate coefficients for H-atom abstraction from several alkanes and alkenes by NO_2 at the CCSD(T)-F12a/cc-pVTZ-f12//B2PLYPD3/cc-pVTZ level of theory. Wang et al. [16] calculated the H-atom abstraction from n-decane by NO_2 at CBS-QB3//M06–2X/6–311++G (d,p) level of theory. More recently, Wu et al. [17] determine the rate coefficients for H-atom abstractions by NO_2 from C_2-C_5 alkanes and alkenes at the DLPNO-CCSD(T)/cc-pVDZ//M06–2X/6−311++g(d,p) level of theory. Nevertheless, there are no theoretical studies on H-atom abstractions by NO_2 from alkynes, dienes and triene. As a result, these reactions are typically missing in existing chemistry models or the rate coefficients are defined by analogy from alkanes and alkenes, leading to large uncertainties in model predictions. Although Ohta et al. [18] measured the rate coefficients of reactions between NO_2 and 16 conjugated alkanes. The reported rate coefficients were combined rate coefficients without information on reaction products or reaction sites.

Therefore, the aims of this study are threefold: (a) conducting a detailed theoretical

investigation of H-atom abstractions from C_3-C_7 alkynes, dienes and triene by NO_2 that form HNO_2, TRANS_HONO and CIS_HONO, via quantum chemistry computation and statistical rate theories; (b) reveal the branching ratios of the three pathways forming the three HNO_2 isomers for the selected species at different H-atom sites and different size of molecules; and (c) systematically analyze the effects of these reactions on model performance and the underlying kinetics.

2. Computational methods

2.1. Potential energy surfaces

Electronic geometries, vibrational frequencies and zero-point energies for all species involved in the 24 reactions (including reactants, products, complexes, transition states (TS's)) are calculated at the M06-2X method [19] coupled with the 6-311++G(d,p) basis set [20-22]. The M06-2X method is well-suited for main-group thermochemistry, kinetics, noncovalent interactions, and electronic excitation energies for both valence and Rydberg states. Moreover, it is parametrized only for nonmetals [19]. The 6-311++G(d,p) basis set is chosen for its balance between accuracy and computational efficiency, providing a good description of electron density with diffuse and polarization functions, which is especially useful in transition state calculations where electron redistribution is important. Conformer search at the same level of theory is conducted to ensure the optimized structures retain the lowest energy. Intrinsic reaction coordinate (IRC) calculations have been carried out at the same level of theory to ensure that the transition state connects the respective reactants with the respective product complex. 1-D hindered rotor treatment [23] are also obtained at the M06–2X/6–311++G(d, p) level of theory for the low frequency torsional modes between non-hydrogen atoms in all of the reactants, TS's, complexes and products, with a total of 18 scans (i.e., 20 degrees increment in the respective dihedral angle) for each rotor. Scale factors of 0.983 for harmonic frequencies

and 0.9698 for ZPEs that were recommended by Zhao and Truhlar [19] are used herein. Single-point energies (SPEs) are further determined for all the species using the DLPNO-CCSD(T) functional [24-25] with the cc-pVDZ basis set. This method has been validated by Yang et al. [26], where it was compared to the more computationally expensive QCISD(T)/CBS level of theory. The results show that the DLPNO-CCSD(T)//cc-pVDZ method yields negligible differences compared to QCISD(T)/CBS in calculating the SPEs of H-atom abstraction reactions, despite the latter being more accurate and computationally demanding. With the CCSD(T) method, attention must be addressed to T1 diagnostic [27] to measure the multi-reference effect. The T1 diagnostic values for all the species, as summarized in Table S1 in the Supplementary Material, are below 0.029, which indicates that the SPEs calculated from using single-reference calculation method are reliable in this study. All the calculations mentioned above are performed using ORCA 5.0.4 [28], and the optimized structures and corresponding graphics for all species, TS's and complexes are summarized in the Supplementary Material.

2.2. Rate constant calculations

The Master Equation System Solver (MESS) program suite [29] is employed here to calculate the chemical rate coefficients for complex-forming reactions via solution of the one-dimensional master equation, based on the chemically significant eigenstate approach of Miller and Klippenstein [30] and the bimolecular species model of Georgievskii and Klippenstein [31]. The frequencies of lower-frequency modes are replaced by the hindered rotor potentials obtained from 1-D scans. Quantum mechanical tunneling corrections assuming the asymmetric Eckart potential (TST/Eck) [32] are applied to obtain the rate coefficient over the temperature range of 298–2000 K. All rate coefficients were fitted to the modified Arrhenius equation, which can be defined as $k = AT^n \exp(-E_a/RT)$.

2.3. Kinetic modeling

The latest chemistry model developed by LLNL [33] is used herein to investigate the influence caused by these calculated reactions on the model performance in predicting combustion characteristics of alkynes, dienes and triene. The development of the chemistry model has been documented in [33], hence will not be presented here. To better represent the benchmark kinetics, the rate coefficients of the H-atom abstraction reactions by $CH_3\dot{O}$ and $CH_3O\dot{O}$ radicals have also been updated following recent studies [34-35]. Kinetic modeling of fundamental combustion experiments, namely autoignition experiments, are completed using the LLNL-developed fast solver Zero-RK [36].

3. Results and discussion

3.1. Species and reaction sites

This study involves three alkynes (C_3H_4, C_4H_6_1, and C_5H_8), four dienes (C_4H_6_13, C_5H_8_13, C_5H_8_14, and C_6H_{10}), and one triene (C_7H_{10}). Each species can undergo H-atom abstraction by NO_2 to form three HNO_2 isomers (TRANS_HONO, HNO_2, and CIS_HONO), encompassing a total of 24 reactions. To better illustrate these reactions, the reaction sites for each species are marked in Fig. 1. According to the type of C-atoms to which H-atoms bond, the reaction sites are divided into primary (P), secondary (S), and tertiary (T) sites. Additionally, reaction sites are designated as α and β according to the proximity to the functional group, while those located at C=C bonds are defined as ν.

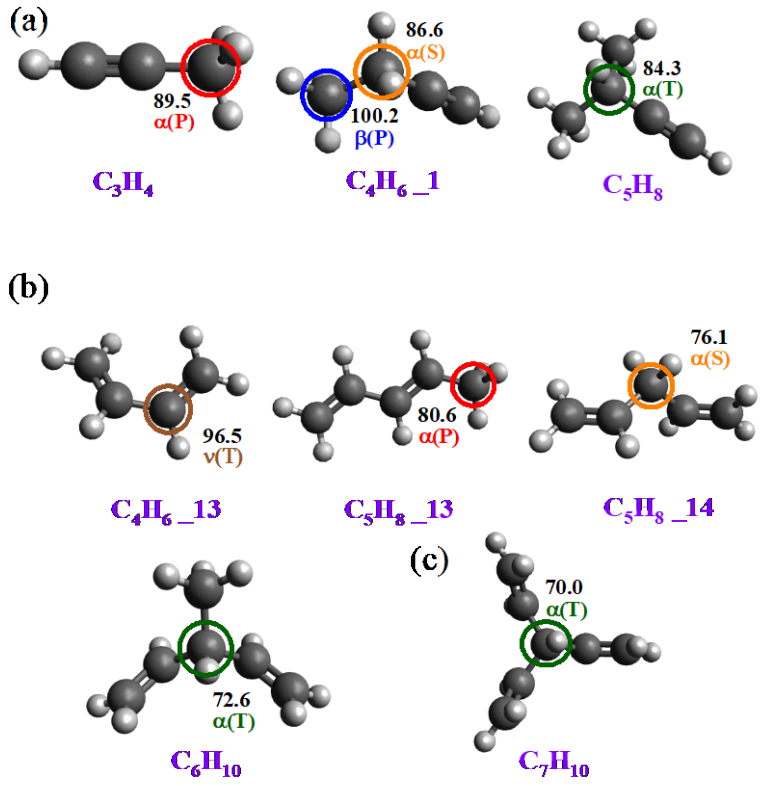

Figure 1. Different abstraction sites and bond dissociation energies (*kcal/mol*) at 0K studied in this study: (a) alkynes, (b) dienes and (c) triene.

Furthermore, C-H bond dissociation energies (BDEs) for different reaction sites at 0 K are also calculated via

$$BDE_0(R-H) = \Delta H^0_{f,0}(\dot{R},g) + \Delta H^0_{f,0}(\dot{H},g) - \Delta H^0_{f,0}(RH,g)$$

As can be seen in Fig. 1a, the BDEs at different sites of alkynes rank as follows, from highest to lowest: β(P) > α(P) > α(S) > α(T), with differences between the P, S, and T sites less than 6 kcal/mol. Notably, the BDE of the β(P) site in C_4H_6_1 is significantly higher than that of the α(P) site in C_3H_4 by approximately 10.7 kcal/mol, highlighting significant impact of

functional groups on BDE. For dienes (as shown in Fig. 1b), the BDE at α-carbons is the highest at the P site (80.6 kcal/mol), followed by the S site (76.1 kcal/mol), and then the T sites (72.6 kcal/mol). Compared to the α-carbon sites, the ν site requires even higher energy to break the C-H bond, with a notable difference of about 16 kcal/mol. For triene, the BDE at α(T) site is lower than that of the diene, which underscores the additional C=C bond in the triene reduces its BDE.

3.2. Electronic energy barriers

The potential energy surfaces (PES) for H-atom abstractions by NO_2 from C_5H_8 and C_5H_8_14 are illustrated in Fig. 2a and Fig. 2b, respectively. These figures also include all related product complexes (PCs) that TS's with the final products. The optimized structures of the TS's are also displayed. Notably, the energy barriers associated with forming TRANS_HONO are consistently the highest among the three channels, which is followed by CIS_HONO and then HNO_2. Mebel et al. [37] attributed this phenomenon to the unique interaction between NO_2 and the H atom to form TRANS_HONO, during which the ON π bond on NO_2 is disrupted, and the unpaired electron is shifted to the oxygen atom to participate in the formation of the O···H bond. This rearrangement increases repulsive interactions between NO_2 and the fuel molecule, thereby elevating the energy barrier for TRANS_HONO formation. Similarly, Chai et al. [15] suggest that the high energy barrier for the TRANS_HONO pathway primarily stems from the need for the RH fragment to approach NO_2 more closely. This is necessary to achieve sufficient orbital overlap without cancellation, which in turn leads to heightened Coulombic repulsion. The PES for all other species involved in this study exhibit

the same trends as those observed in Fig. 2, which are presented in Figs. S1-S2 in the Supplementary Material.

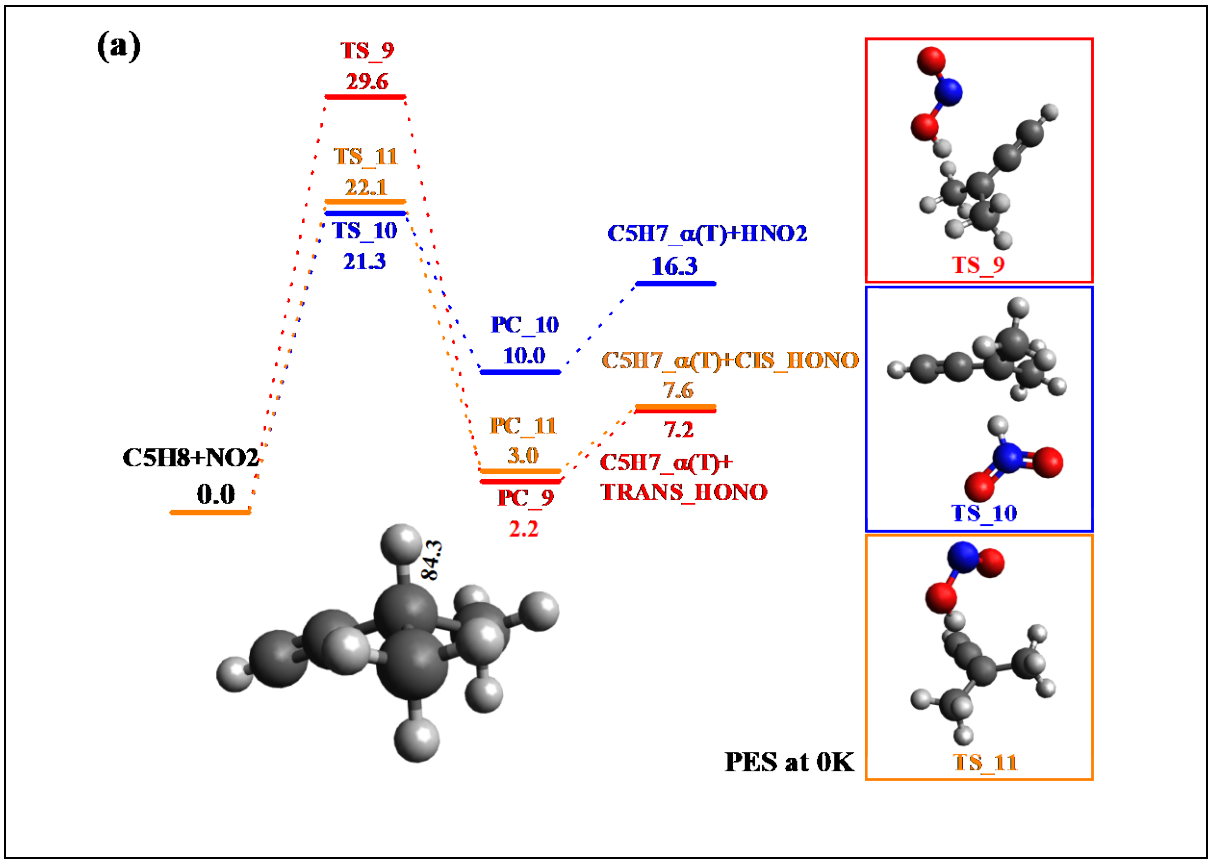

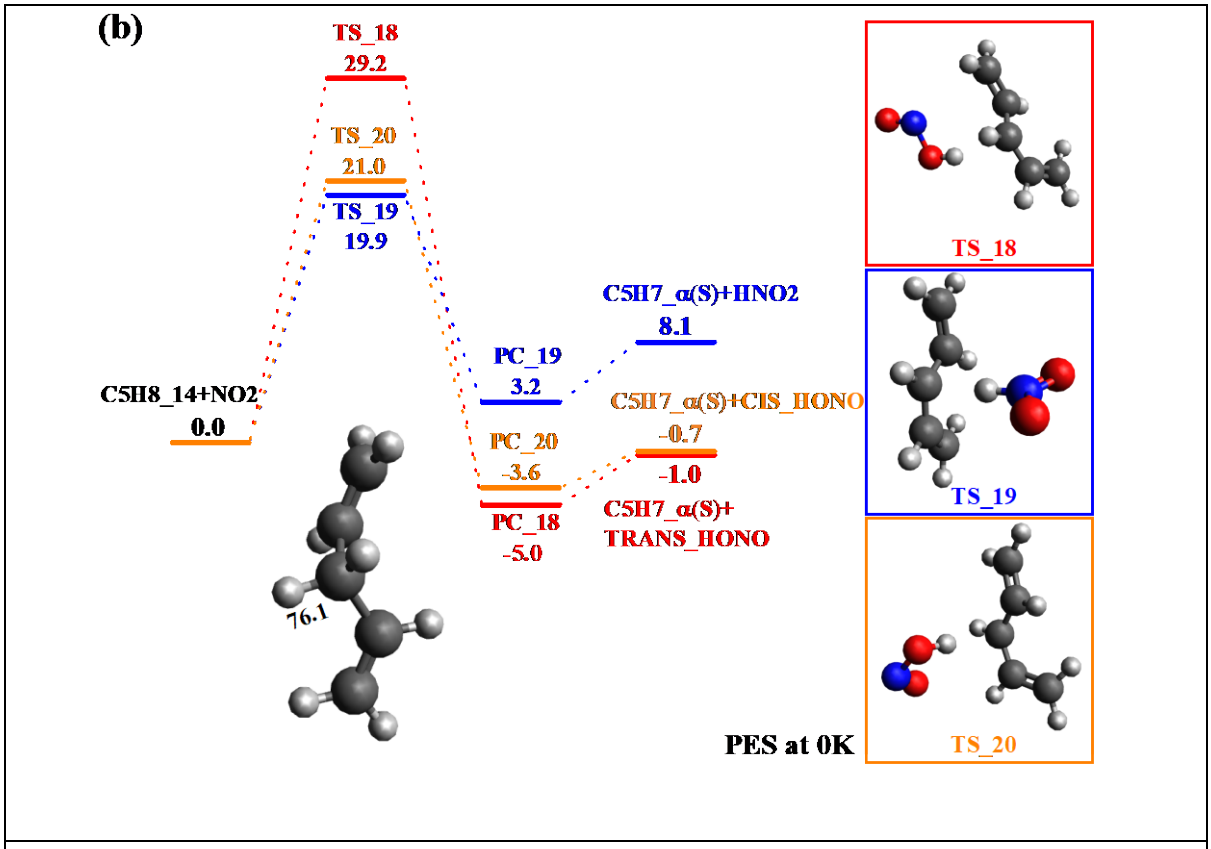

Figure 2. The PES for H-atom abstraction by NO_2 from (a) C_5H_8 to form C_5H_7_α(T) and (b) C_5H_8_14 to form C_5H_7_α(S) at 0K. Energies are quantified in kcal/mol. Additional products include TRANS_HONO (indicated by a red line), HNO_2 (blue line), and CIS_HONO (orange line). Side boxes highlight the structure of transition state for different pathways.

191

192 Table 1 The relative energy for H-atom abstraction by NO_2 from different sites of alkynes and
193 dienes to form the respective products and HNO_2 isomers (TRANS_HONO, HNO_2,
194 CIS_HONO) at 0K. All values are in kcal/mol.

No.	Reaction	Reactant	TS	Product complex	Product
	Alkynes + NO_2				
R1	$C_3H_4+NO_2 \rightarrow C_3H_3$_α(P)+TRANS_HONO	0	34.4	8.4	12.4
R2	$C_3H_4+NO_2 \rightarrow C_3H_3$_α(P)+$HNO_2$	0	27.4	17.5	21.5
R3	$C_3H_4+NO_2 \rightarrow C_3H_3$_α(P)+CIS_HONO	0	27.4	9.0	12.8
R4	C_4H_6_1+$NO_2 \rightarrow C_4H_5$_β(P)+TRANS_HONO	0	32.8	21.1	23.1
R5	C_4H_6_1+$NO_2 \rightarrow C_4H_5$_β(P)+HNO_2	0	31.2	27.5	32.2
R6	C_4H_6_1+$NO_2 \rightarrow C_4H_5$_β(P)+CIS_HONO	0	29.4	20.8	23.5
R7	C_4H_6_1+$NO_2 \rightarrow C_4H_5$_α(S)+HNO_2	0	24.0	13.3	18.6
R8	C_4H_6_1+$NO_2 \rightarrow C_4H_5$_α(S)+CIS_HONO	0	24.0	6.2	9.8
R9	$C_5H_8+NO_2 \rightarrow C_5H_7$_α(T)+TRANS_HONO	0	29.6	2.2	7.2

R10	$C_5H_8+NO_2 \rightarrow C_5H_7\_\alpha(T)+HNO_2$	0	21.3	10.0	16.3
R11	$C_5H_8+NO_2 \rightarrow C_5H_7\_\alpha(T)+CIS\_HONO$	0	22.1	3.0	7.6
	Dienes + NO_2				
R12	$C_4H_6\_13+NO_2 \rightarrow C_4H_5\_\nu(T)+TRANS\_HONO$	0	35.3	15.1	19.4
R13	$C_4H_6\_13+NO_2 \rightarrow C_4H_5\_\nu(T)+HNO_2$	0	30.7	23.9	28.5
R14	$C_4H_6\_13+NO_2 \rightarrow C_4H_5\_\nu(T)+CIS\_HONO$	0	29.7	16.0	19.7
R15	$C_5H_8\_13+NO_2 \rightarrow C_5H_7\_\alpha(P)+TRANS\_HONO$	0	29.4	-0.6	3.5
R16	$C_5H_8\_13+NO_2 \rightarrow C_5H_7\_\alpha(P)+HNO_2$	0	22.3	8.2	12.6
R17	$C_5H_8\_13+NO_2 \rightarrow C_5H_7\_\alpha(P)+CIS\_HONO$	0	23.5	0.5	3.9
R18	$C_5H_8\_14+NO_2 \rightarrow C_5H_7\_\alpha(S)+TRANS\_HONO$	0	29.2	-5.0	-1.0
R19	$C_5H_8\_14+NO_2 \rightarrow C_5H_7\_\alpha(S)+HNO_2$	0	19.9	3.2	8.1
R20	$C_5H_8\_14+NO_2 \rightarrow C_5H_7\_\alpha(S)+CIS\_HONO$	0	21.0	-3.6	-0.7
R21	$C_6H_{10}+NO_2 \rightarrow C_6H_9\_\alpha(T)+TRANS\_HONO$	0	27.3	-8.9	-4.4
R22	$C_6H_{10}+NO_2 \rightarrow C_6H_9\_\alpha(T)+HNO_2$	0	16.9	0.1	4.6
	Triene + NO_2				
R23	$C_7H_{10}+NO_2 \rightarrow C_7H_9\_\alpha(T)+TRANS\_HONO$	0	26.9	-10.9	-7.1
R24	$C_7H_{10}+NO_2 \rightarrow C_7H_9\_\alpha(T)+HNO_2$	0	16.4	-2.7	1.9

Table 1 presents a detailed analysis of the reactive energies, hence energy barriers, associated with H-atom abstractions from alkynes, dienes and triene that are determined from the PES. The relative energies are calculated as the absolute energies subtracting the energies of the respective reactants at 0K. With this treatment, the relative energy of the TS indicates the energy barrier for that specific H-atom abstraction reaction. For alkynes, energy barrier for reactions yielding the same HNO_2 product generally follow a similar trend as that observed with the BDEs in Fig. 1, following the order of β(P) > α(P) > α(S) > α(T). The energy barrier for the reactions forming TRANS_HONO is consistently higher than the other two counterparts. In dienes, the potential energy at the ν site for forming transition states is significantly higher than those at the α site. Specifically, the energies required to form TRANS_HONO, HNO_2, and CIS_HONO at the ν sites (i.e., from C_4H_6) are 35.3 kcal/mol, 30.7 kcal/mol, and 29.7 kcal/mol,

207 respectively. In contrast, at the α site, the energies (averaged from C_5H_8 and C_6H_{10}) for forming
208 TRANS_HONO, HNO_2, and CIS_HONO are approximately 28 kcal/mol, 19 kcal/mol, and 22
209 kcal/mol, respectively. Additionally, by comparing the energy barriers between C_6H_{10} and
210 C_7H_{10}, it can be seen that the energy barriers at the same site differ by less than 0.5 kcal/mol.
211 Therefore, the additional C=C bond in C_7H_{10} has a minimal effect on the energy barriers
212 compared to C_6H_{10}.

213 *3.3. Rate constants and rate rules*

214 The rate coefficients for H-atom abstraction by NO_2, fitted into the Arrhenius expression,
215 are summarized in Table 2. The rate coefficients forming different products at the same reaction
216 site, in the temperature range of 298 – 2000 K, are illustrated in Figs. S3 – S4 in the
217 Supplementary Material. In all the cases, the rate coefficient for the reaction forming
218 TRANS_HONO is consistently smaller in the low temperature range, which is consistent with
219 the energy barrier shown in Table 1. This difference decreases with increasing temperature.

220 Table 2 The rate coefficient for H-atom abstraction by NO_2 from alkynes and dienes to form
221 the respective products and HNO_2 isomers (TRANS_HONO, HNO_2, CIS_HONO).

No.	Reaction	A (cm^3/mol*s)	n	Ea (cal/mol)
	Alkynes + NO_2			
R1	$C_3H_4+NO_2 \rightarrow C_3H_3\_\alpha(P)+TRANS\_HONO$	1.000E+00	3.707	28054.10
R2	$C_3H_4+NO_2 \rightarrow C_3H_3\_\alpha(P)+HNO_2$	1.000E+00	3.795	23170.45
R3	$C_3H_4+NO_2 \rightarrow C_3H_3\_\alpha(P)+CIS\_HONO$	1.000E+00	3.795	21896.31
R4	$C_4H_6\_1+NO_2 \rightarrow C_4H_5\_\beta(P)+TRANS\_HONO$	1.001E+00	3.933	30464.77
R5	$C_4H_6\_1+NO_2 \rightarrow C_4H_5\_\beta(P)+HNO_2$	1.001E+00	3.795	28695.59
R6	$C_4H_6\_1+NO_2 \rightarrow C_4H_5\_\beta(P)+CIS\_HONO$	1.001E+00	3.964	25809.74
R7	$C_4H_6\_1+NO_2 \rightarrow C_4H_5\_\alpha(S)+HNO_2$	1.001E+00	3.603	19932.70
R8	$C_4H_6\_1+NO_2 \rightarrow C_4H_5\_\alpha(S)+CIS\_HONO$	1.001E+00	3.689	19811.52
R9	$C_5H_8+NO_2 \rightarrow C_5H_7\_\alpha(T)+TRANS\_HONO$	1.001E+00	3.650	25086.67
R10	$C_5H_8+NO_2 \rightarrow C_5H_7\_\alpha(T)+HNO_2$	1.001E+00	3.640	17215.96
R11	$C_5H_8+NO_2 \rightarrow C_5H_7\_\alpha(T)+CIS\_HONO$	1.001E+00	3.926	18231.40

	Dienes + NO_2			
R12	C_4H_6_13+NO_2→C_4H_5 _ν(T)+TRANS_HONO	1.001E+00	3.938	32565.68
R13	C_4H_6_13+NO_2→C_4H_5 _ν(T)+HNO_2	1.002E+00	3.933	27257.57
R14	C_4H_6_13+NO_2→C_4H_5 _ν(T)+CIS_HONO	1.000E+00	4.030	25063.31
R15	C_5H_8_13+NO_2→C_5H_7 _α(P)+TRANS_HONO	1.001E+00	3.317	23831.78
R16	C_5H_8_13+NO_2→C_5H_7 _α(P)+HNO_2	1.001E+00	3.453	17667.69
R17	C_5H_8_13+NO_2→C_5H_7 _α(P)+CIS_HONO	1.001E+00	3.529	18625.16
R18	C_5H_8_14+NO_2→C_5H_7 _α(S) +TRANS_HONO	1.001E+00	3.383	24153.35
R19	C_5H_8_14+NO_2→C_5H_7 _α(S)+HNO_2	1.001E+00	3.641	15693.22
R20	C_5H_8_14+NO_2→C_5H_7 _α(S)+CIS_HONO	1.000E+00	3.466	17517.12
R21	C_6H_{10}+NO_2→C_6H_9 _α(T)+TRANS_HONO	1.001E+00	3.257	22743.76
R22	C_6H_{10}+NO_2→C_6H_9 _α(T)+ HNO_2	1.001E+00	3.497	12451.33
	Triene + NO_2			
R23	C_7H_{10}+NO_2→C_7H_9 _α(T)+TRANS_HONO	1.001E+00	3.250	22241.79
R24	C_7H_{10}+NO_2→C_7H_9 _α(T)+HNO_2	1.001E+00	3.423	11807.62

Figure 3 illustrates the rate coefficients for H-atom abstraction by NO_2 from alkynes forming different products. For the reactions forming TRANS_HONO (Fig.3a), the difference in rate coefficients among all species is within four orders of magnitude at 298K, which narrows down to approximately one magnitude order at 2000K. The rate coefficient at the P sites is lower than that at the T site, regardless of the proximity to the triple bond. On the other hand, as depicted in Figs. 3b and 3c, the rate coefficients at low temperatures for reactions forming both HNO_2 and CIS_HONO show substantial differences between different reaction sites. The highest rate coefficients are observed for the reaction of C_5H_8 forming C_5H_7_α(T), followed in descending order by C_4H_6_1 to C_4H_5_α(S), C_3H_4 to C_3H_3_α(P), and lastly, C_4H_6_1 to C_4H_5_β(P). Notably, the rate coefficients for C_4H_6_1 at the β(P) site are significantly lower than those at the α(P) site, which differs from the trends observed in Fig. 3a. Furthermore, the rate coefficient between C_4H_6_1 forming C_4H_5_α(S) and C_3H_4 forming C_3H_3_α(P) differs by approximately two orders of magnitude, which quickly diminishes as temperature increases.

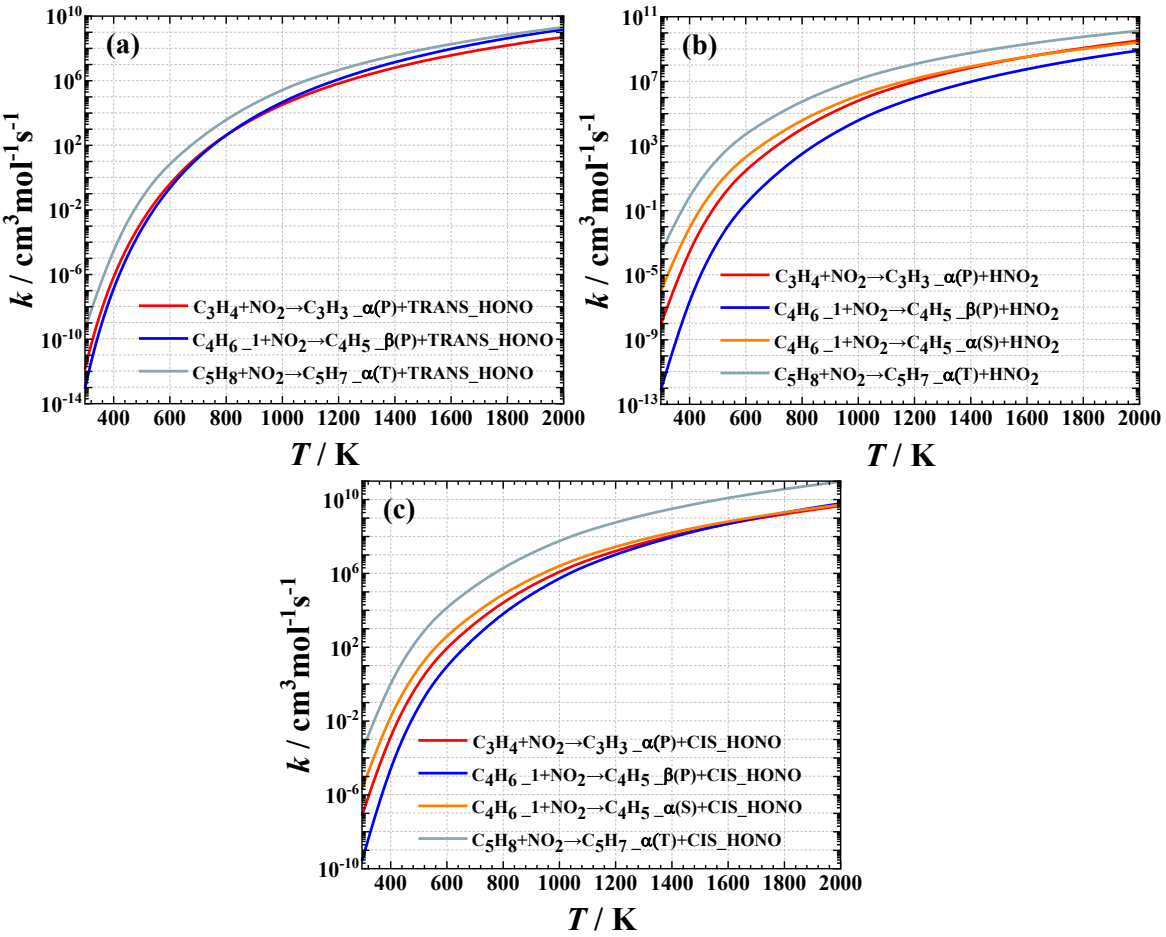

Figure 3. The comparison between the rate coefficients for H-atom abstraction by NO_2 from alkynes to form (a) TRANS_HONO, (b) HNO_2, and (c) CIS_HONO. Data are presented on per H atom basis.

236

237 Figure 4 focuses on comparing the rate coefficients for H-atom abstraction by the NO_2

238 from dienes and tirene. It is obvious from Figs. 4a and 4b that the rate coefficients for C_6H_{10}

239 forming C_6H_9_α(T) closely mirror those for C_7H_{10} forming C_7H_9_α(T) across the temperature

240 range studied, highlighting the consistent rate rules at the same reaction site among species of

241 different sizes. Furthermore, it demonstrates that dienes and triene exhibit similar rate

242 coefficients at the same reaction sites, indicating structural similarities in their H-abstraction

behavior. At low temperatures, the rate coefficients are ranked from highest to lowest as follows: α(T) > α(S) > α(P) > ν(T). This sequence highlights the significant influence of reaction sites on the rate of H-atom abstraction. Furthermore, as can be seen in Fig. 4a, the rate coefficient for C_5H_8_13 forming C_5H_7_α(P) is slightly lower than that for C_5H_8_14 forming C_5H_7_α(S), primarily due to a small difference in energy barriers between these two reactions, which is around 0.2 kcal/mol (c.f. Table 1). As temperature increases, the difference in rate coefficients across all reactions diminishes. Nevertheless, it is worth noting that the rate coefficient for C_4H_6_13 forming C_4H_5_ν(T) dramatically increases with temperature, ultimately becoming the highest or nearly the highest among all reactions at 2000K. This could be due to the enhanced influences of hindered rotor effects at higher temperatures. Comparison between the rate coefficients for H-atom abstraction by NO_2 radical from different sites on the same molecule has also been conducted for C_4H_6_1 (as can be seen in Fig. S5), where the rate coefficient at the β(P) site is always several magnitudes lower than that at the α(S) site.

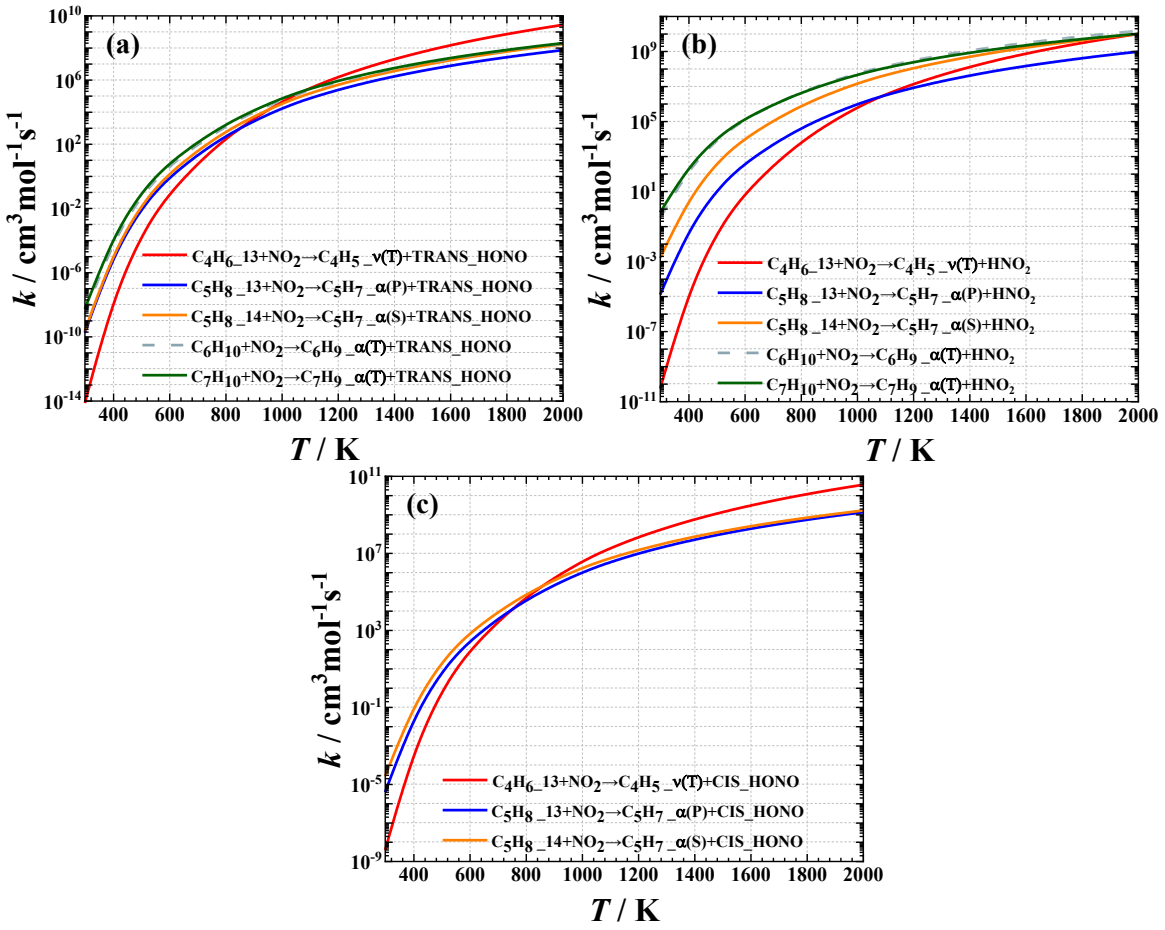

Figure 4. The comparison between the rate coefficients for H-atom abstraction by NO_2 from dienes and triene to form (a) TRANS_HONO, (b) HNO_2, and (c) CIS_HONO. Data are presented on per H atom basis.

256

257 *3.4. Rate constants and branching ratios*

258 Figure 5 illustrates the branching ratios for H-atom abstraction by the NO_2 from alkynes
259 to form HNO_2 isomers. Immediately seen in Fig. 5 is the dominancy of the CIS_HONO channel,
260 which exhibits a branching ratio that is considerably higher than the other two channels. This
261 is most obvious for C_4H_6 (Fig. 5b) where the branching ratio for the CIS_HONO channel
262 reaches nearly 1 at below 400 K. Differences are also observed between the three alkynes.

Specifically, the branching ratios for CIS_HONO at the α-P site of C_3H_4 and the β-P site of C_4H_6 decrease with rising temperatures, as seen in Figs. 5a and 5b, respectively, whereas that at the α-T site of C_5H_8 increases with temperature, Fig. 5c. Consequently, the dependence of branching ratio on temperature for the HNO_2 channel also displays opposite trends between the α-T site C_5H_8 and the other two sites of C_3H_4 and C_4H_6. Notably, for HNO_2, the branching ratio increases significantly for C_3H_4 at the α-P site from about 10% to 40% as the temperature rises to 2000 K, while for C_4H_6 at the β-P site, it falls below that of TRANS_HONO, stabilizing at around 10%. Across all species, the proportions of TRANS_HONO remain relatively low, typically not exceeding 20%, indicating that this pathway is less favored compared to the pathways forming CIS_HONO and HNO_2.

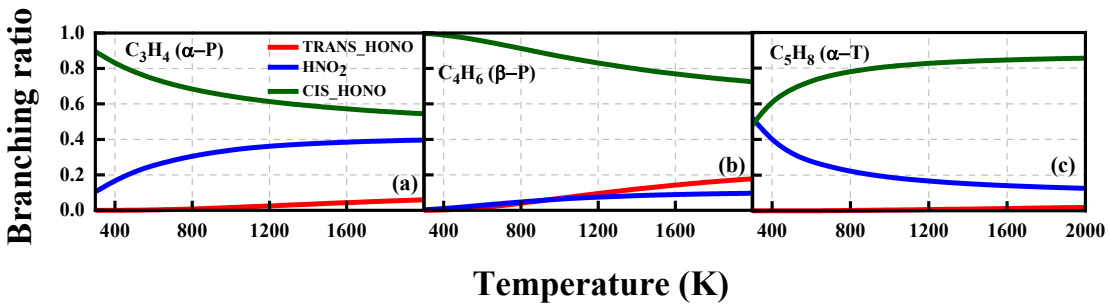

Figure 5. The comparison between the branching ratio for H-atom abstraction by NO_2 from alkynes to form HNO_2 isomers (TRANS_HONO, HNO_2, CIS_HONO), (a) C_3H_4(α-P), (b) C_4H_6(β-P), (c) C_5H_8(α-T).

Figure 6 further shows the branching ratios for H-atom abstraction by the NO_2 from dienes. These branching ratios correlate closely with the corresponding energy barriers in Table 1. For instance, the branching ratios of CIS_HONO and HNO_2 for C_5H_8_13 at the α-P site intersect at approximately 870K, as illustrated in Fig. 6b and the rate coefficients for these reactions also intersect at this temperature (see Fig. S4b). This intersection highlights a critical temperature

where the preferential formation of the HNO_2 isomers shifts. The trends of branching ratio at the ν-T site of C_4H_6_13 are similar to those observed in Fig. 5, where the CIS_HONO channel is the most dominant. However, a closer observation of Fig. 6 highlights the considerably different branching ratios at the α site between alkynes (Figs. 5a and 5c) and dienes (Figs. 6b and 6c). Specifically, at the α site of dienes, the branching ratio is mostly favored toward the HNO_2 channel, rather than the CIS_HONO channel as observed for alkynes. The TRANS_HONO channel is consistently the least important for both alkynes and dienes.

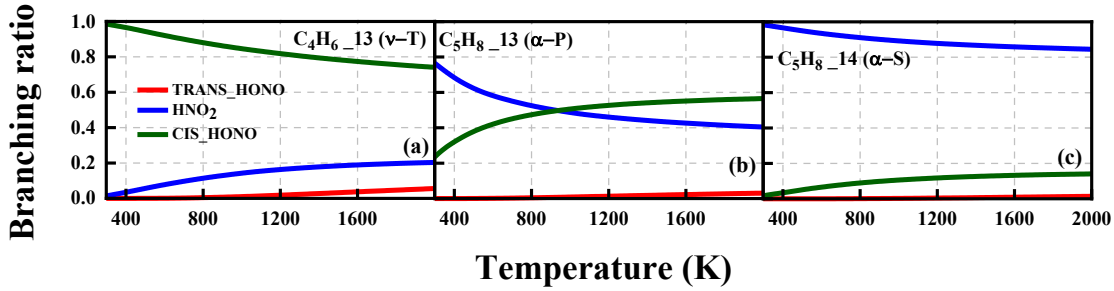

Figure 6. The comparison between the branching ratio for H-atom abstraction by NO_2 from dienes to form HNO_2 isomers (TRANS_HONO, HNO_2, CIS_HONO), (a) C_4H_6_13 (ν-T), (b) C_5H_8_13 (α-P), (c) C_5H_8 _14(α-S).

Figure 7 illustrates the branching ratios of alkynes and dienes versus carbon number across various temperatures. At 600 K (Fig. 7a), the branching ratio for CIS_HONO starts at about 75% for alkynes with three carbon atoms, increases to approximately 97% for those with four carbon atoms, and then decreases slightly to about 70% for five carbon atoms. In contrast, the branching ratio for HNO_2 displays a reversed trend. These trends are consistent at different temperatures, as depicted in Figs. 7b – 7d. Greater shifts in branching ratio cross different carbon atom numbers are observed for dienes (Fig. 7 – right panel). However, when the carbon

count increases to five, the trend reverses, with the branching ratio of CIS_HONO falling below that of HNO_2.

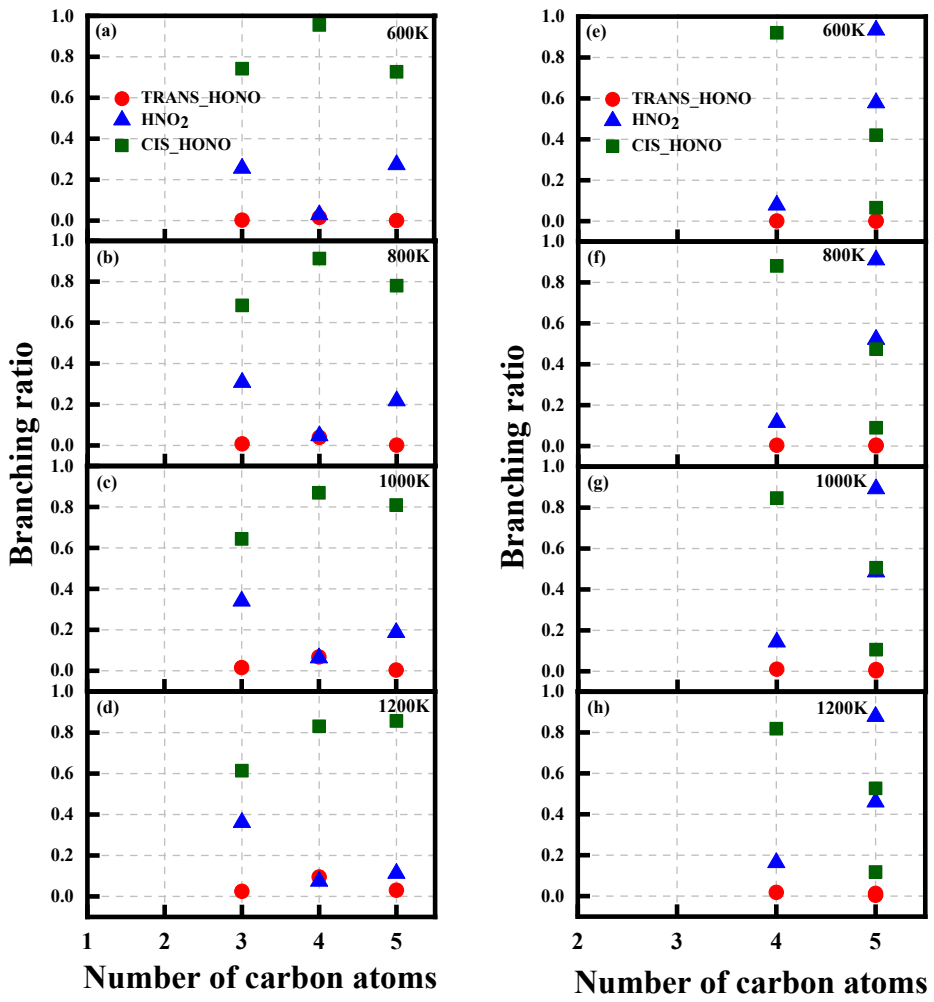

Figure 7. Branching ratio of alkynes (left panel) and dienes (right panel) versus carbon number at 600K ((a)&(e)), 800K ((b)&(f)), 1000K ((c)&(g)) and 1200K ((d)&(h)).

3.5. Model implementations and implications

To investigate the influences of the studied reactions on model predictions, the calculated rate parameters are incorporated individually for each species into the detailed gasoline surrogate chemistry model [33]. The model without and with the updated rate parameters is

300 referred to as “original model” and “updated model” in the following. It should be noted that
301 the purpose of model implementations is to illustrate the impact of the calculated reactions,
302 rather than to propose a new model. The experimental conditions from [14] are adopted, where
303 a rapid compression machine was used to study the interactions between NO_x and unsaturated
304 hydrocarbons with strong NO_x blending effects on ignition propensity observed.

305 Figure 8 compares the simulated ignition delay times (IDTs) between the original and
306 updated models for alkynes. It can be seen that the original model and the updated model show
307 significant differences with greater differences observed at low temperatures, indicating the
308 critical role of the studied reactions in determining model reactivity. Specifically, the updated
309 model becomes more reactive than the original model, advancing the ignition delay time by up
310 to 0.5 magnitude order. Besides, the negative temperature coefficient (NTC) behavior is
311 seemingly weakened in the updated model for C_3H_4, as shown in Fig. 8a.

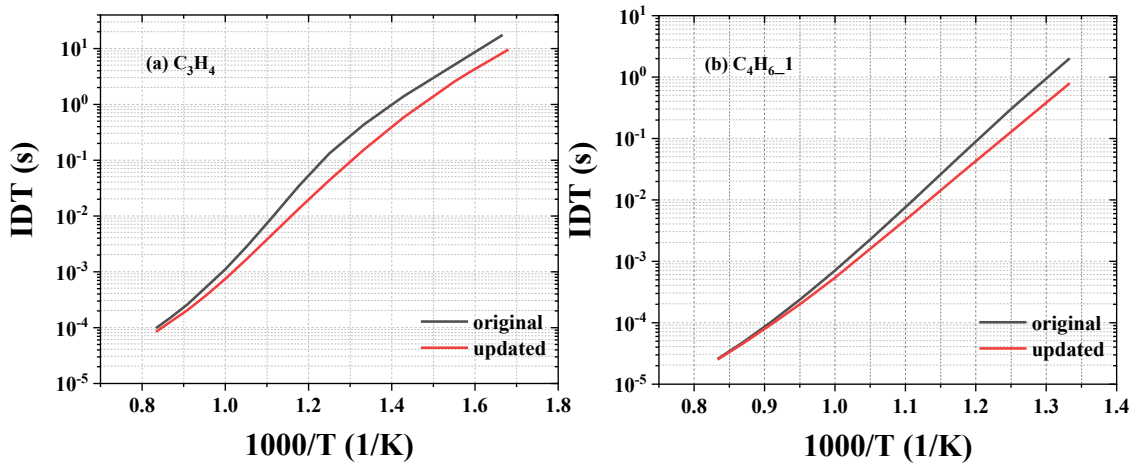

Figure 8. The IDT of alkynes ((a) C_3H_4 and (b) C_4H_6_1) simulated using the original and updated model at pressure of 40 bar, equivalence ratio of 1, temperature range of 600-1200 K, and with 1000 ppm NO_2 doped.

312

Figure 9 shows the comparison of the simulated IDT for dienes between the original and updated models. It is clear from Fig. 9 that the updated rate parameters greatly influence the model prediction results for dienes, highlighting the need to accurately represent these reactions in chemistry models. Similar to the results in Fig. 8, with incorporating the updated rate parameters, the model becomes more reactive, with more pronounced change in model predictions observed for C_4H_6_13 and C_6H_{10} than for C_5H_8_14 and C_5H_8_13. The change in model reactivity is surprisingly large for C_6H_{10} (e.g., IDT advanced by ~2 magnitude orders, as shown in Fig. 9d), indicating that its chemistry was ill-conditioned in the original model and requires further updates.

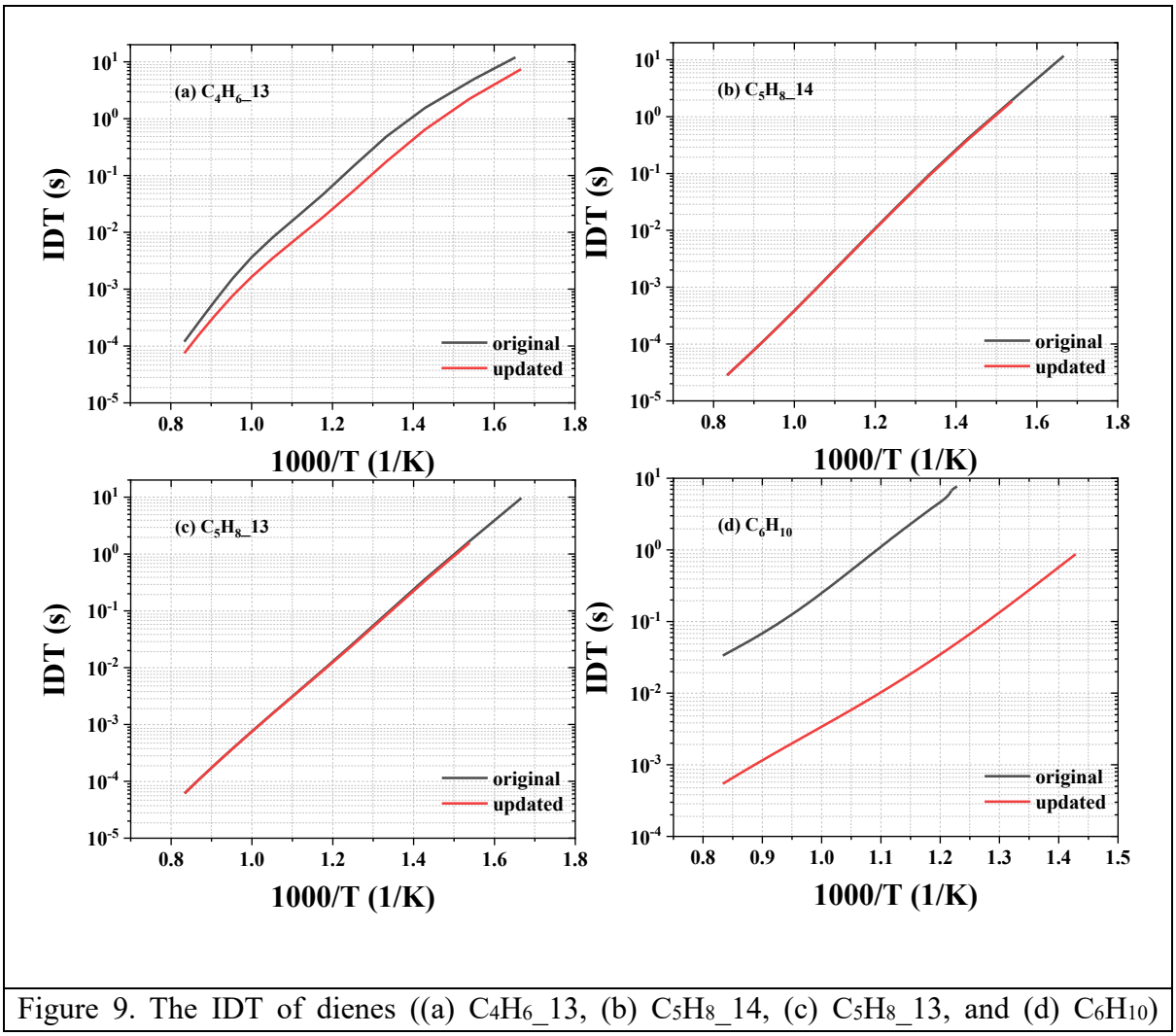

Figure 9. The IDT of dienes ((a) C_4H_6_13, (b) C_5H_8_14, (c) C_5H_8_13, and (d) C_6H_{10})

simulated using the original and updated model at pressure of 40 bar, equivalence ratio of 1, temperature range of 600-1200 K, and with 1000 ppm NO_2 doped.

322

323 To investigate the underlying kinetics governing the model reactivity after incorporating
324 the updated rate parameters, sensitivity analysis is further conducted at the same conditions as
325 in Figs. 8 and 9, but only at two representative temperatures, i.e., 700 and 1100 K. Two
326 representative species, namely C_4H_6_1 for alkynes and C_4H_6_13 for dienes, are selected. The
327 sensitivity analysis coefficient is defined as $S_{rel} = \ln(\frac{\tau^{\Delta}}{\tau})/\ln(\frac{k^{\Delta}}{k})$, where τ^{Δ} is the gas
328 temperature (over the whole ignition delay period) after multiplying the original rate constant
329 by 2, i.e., $k^{\Delta} = 2 * k$, and τ is the original mixture temperature. Negative sensitivity coefficient
330 indicates an inhibiting effect on mixture reactivity, while the positive sensitivity coefficient
331 indicates a promoting effect. The computed sensitivity coefficients for the 16 most sensitive
332 reactions are presented for each mixture at each condition.

333 As shown in Fig. 10a, at 750 K, the sensitivity coefficients computed by the original model
334 are considerably greater than those computed by the updated model, whereas those at 1100 K
335 are quite similar between the original and updated models. This is consistent with the IDT
336 results in Fig. 8b, where the change in predicted IDT between the two models is almost the
337 highest at 750 K while the lowest at 1100 K. Overall, both the promoting and inhibiting effects
338 of the most sensitive reactions at 750 K are suppressed in the updated model, counteracting
339 each other. However, the fifth most sensitive reaction, namely C_4H_6_1+NO_2 =
340 C_4H_5_α(S)+CIS_HONO, displays a strong promoting effect on autoignition reactivity in the
341 updated model, whereas this reaction was not available in the original model. The produced

CIS_HONO quickly decomposes to OH and NO, which further promotes ignition reactivity, as can be seen in Fig. 10a where OH+NO = HONO exhibits a positive sensitivity coefficient. The sensitivity coefficients for OH+NO = HONO remain similar between the updated and original models, which is different from the other reactions. This is primarily due to the increased contribution to HONO production via C_4H_6_1+NO_2 = C_4H_5_α(S)+CIS_HONO. These contributions eventually lead to the increased autoignition reactivity with the updated model. The trends observed at 750 K for C_4H_6_1+NO_2 = C_4H_5_α(S)+CIS_HONO are also observed at 1100 K, but less pronounced, as can be inferred from Fig. 10b.

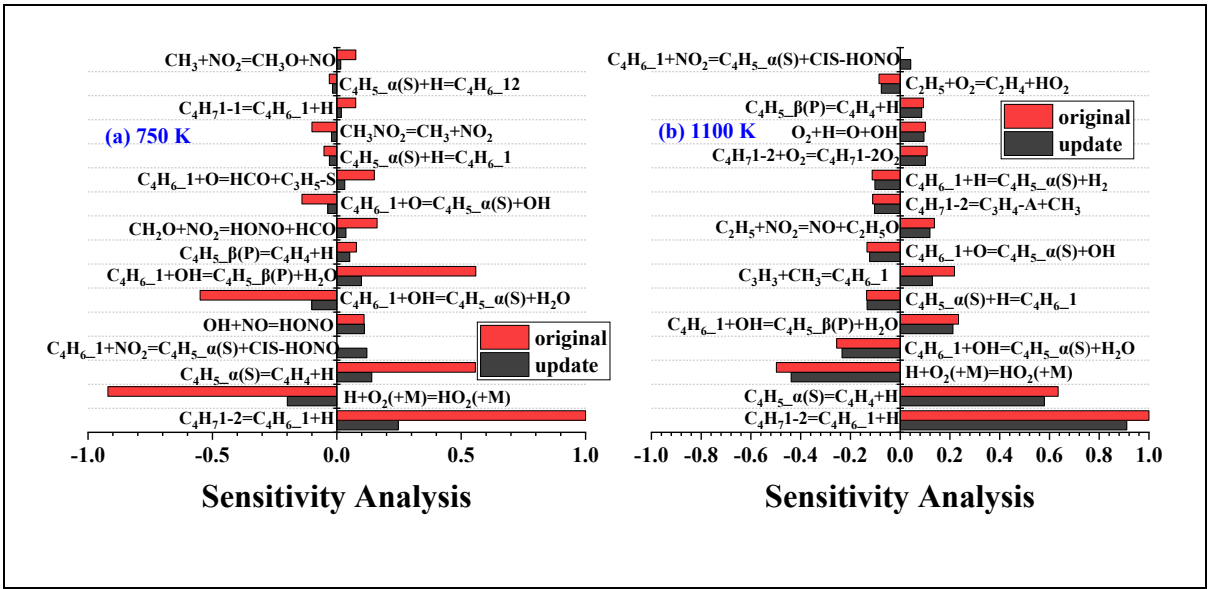

Figure 10. The sensitivity analysis on gas temperature for C_4H_6_1 at P_C=40 bar, equivalence ratio of 1, and with 1000 ppm NO_2 doped. (a) T_C=750 K and (b) T_C=1000 K.

The sensitivity analysis results for C_4H_6_13, as shown in Fig. 11, are somewhat different from those in Fig. 10. First, the difference in sensitivity coefficients between the updated and original models is significant at both 750 K and 1100 K, with relatively higher difference seen at 750 K. This, again, corroborates with the simulated IDT results (c.f., Fig. 9a), where the

updated model shows different autoignition reactivity at both 750 K and 1100 K. Second, apart from the dominant promoting effect from the reaction forming CIS_HONO in the updated model, namely C_4H_6_13+NO_2 = C_4H_5_v(T)+CIS_HONO, there is also a relatively smaller promotion effect from C_4H_6_13+NO_2 = C_4H_5_v(T)+HNO_2. The different levels of contribution from the CIS_HONO and HNO_2 channels are supported by the branching ratios in Fig. 6a where the CIS_HONO channel is consistently the most dominant pathway at all temperatures studied. The promotion effects from these two H-atom abstraction pathways by NO_2 explain the increased autoignition reactivity in the updated model.

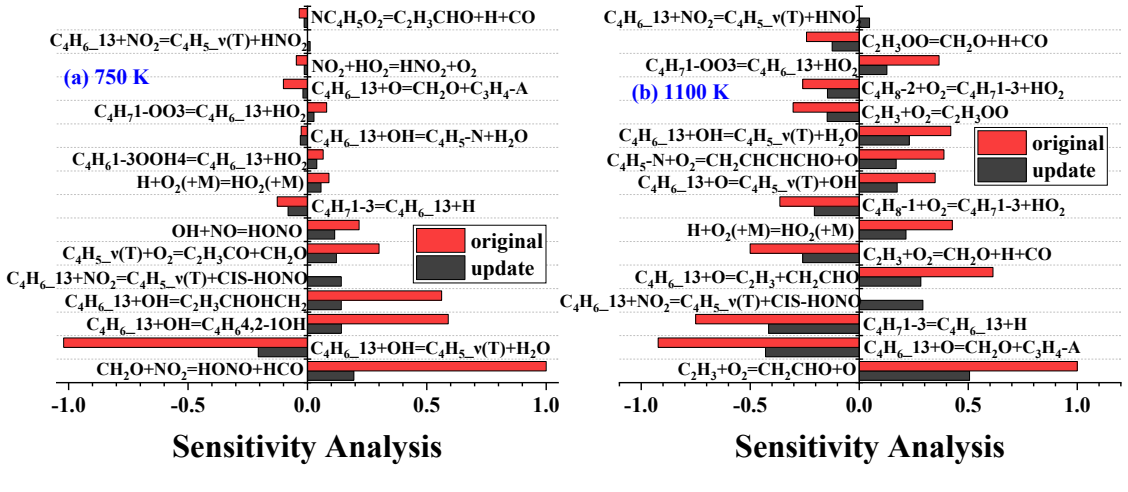

Figure 11. The sensitivity analysis on gas temperature for C_4H_6_13 at P_C=40 bar, equivalence ratio of 1, and with 1000 ppm NO_2 doped. (a) T_C=750 K and (b) T_C=1000 K.

Flux analyses are further conducted at the same conditions as sensitivity analysis at 1% fuel consumption, which are summarized in Figs. 12 and 13 for C_4H_6_1 (alkyne) and C_4H_6_13 (diene). The percentages shown in Figs. 12 and 13 are computed as the ratio of the rate of consumption for that pathway to the total rate of consumption.

As can be seen in Fig. 12, the H atom of C_4H_6_1 is mainly abstracted by OH and H radicals in the original model, leading to the formation of C_4H_5_α(S), C_4H_5_β(P) and $C_4H_7$1-2. However, with the H-atom abstraction reactions by NO_2 incorporated into the updated model, over 30% of C_4H_6_1 is consumed by NO_2 at 750 K, with 29% and 1.4% of C_4H_6_1 reacted to form C_4H_5_α(S) and C_4H_5_β(P), respectively. As a result, C_4H_6_1 consumption by OH is reduced at this temperature, e.g., from 40.2% to 30.5% for the formation of C_4H_5_α(S). As can be seen from Fig. 10a that C_4H_6_1+NO_2 = C_4H_5_α(S)+CIS_HONO is a promoting reaction, while C_4H_6_1+OH = C_4H_5_α(S)+H_2O is an inhibiting reaction. The increased flux in the former reaction and decrease in the later reaction will greatly promote ignition reactivity, as observed in Fig. 8a. The shifts in fluxes for the C_4H_6_1 consuming pathways observed at 750 K are not observed at 1100 K, where the H-atom abstractions by NO_2 show no contributions. Instead, great changes are seen for the consumption of CH_2O and CO, where the flux through the NO_2-involving channel is reduced in the updated model. Nevertheless, these two reactions are not identified as the most sensitive reactions at 1100 K, as shown in Fig. 10b.

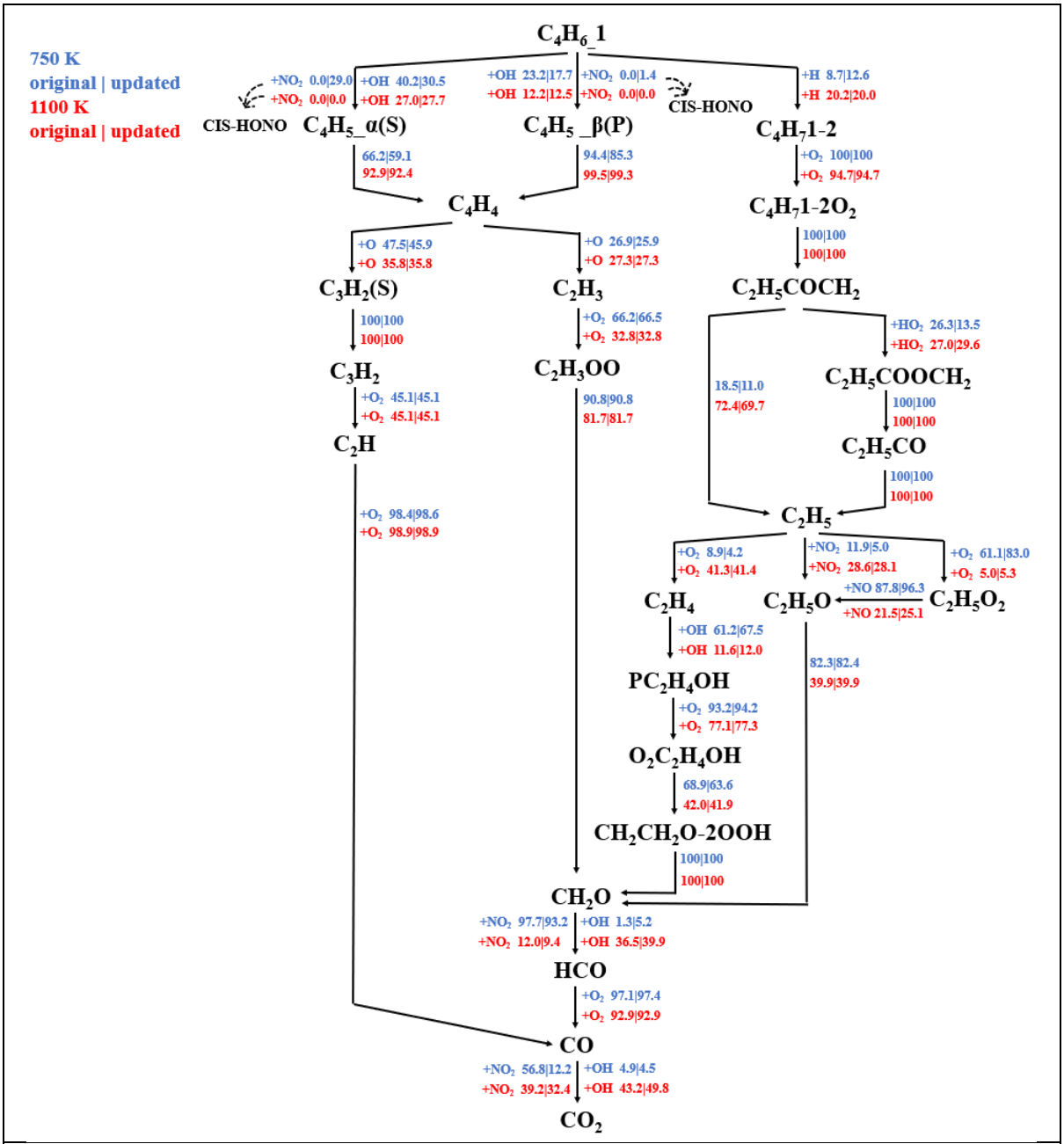

Figure 12. The flux analysis results for C_4H_6_1 ignition at P_C = 40 bar, T_C = 750 and 1100 K, equivalence ratio of 1, and with 1000 ppm NO_2 doped. Fluxes are computed at 1% C_4H_6_1 consumption.

382

383 Similar to the results in Fig. 12, Fig. 13 shows that the consuming pathways of C_4H_6_13

384 shift toward H-atom abstraction by NO_2 forming C_4H_5_v(T) and away from the H-atom

385 abstraction by OH in the updated model at 750 K. This leads to an enhanced promoting effect

386 from C_4H_6_13+NO_2 = C_4H_5_v(T)+CIS_HONO and a suppressed inhibiting effect from

C_4H_6_13+OH = C_4H_5_v(T) (or C_4H_5_N) +H_2O, resulting in an increased model reactivity. Different from Fig. 12, the H-atom abstraction by NO_2 forming C_4H_5_v(T) demonstrates obvious contributions to C_4H_6_13 consumption even at 1100 K. This explains the results in Fig. 11b, where C_4H_6_13+NO_2 = C_4H_5_v(T)+CIS_HONO is still among the top promoting reactions at 1100 K.

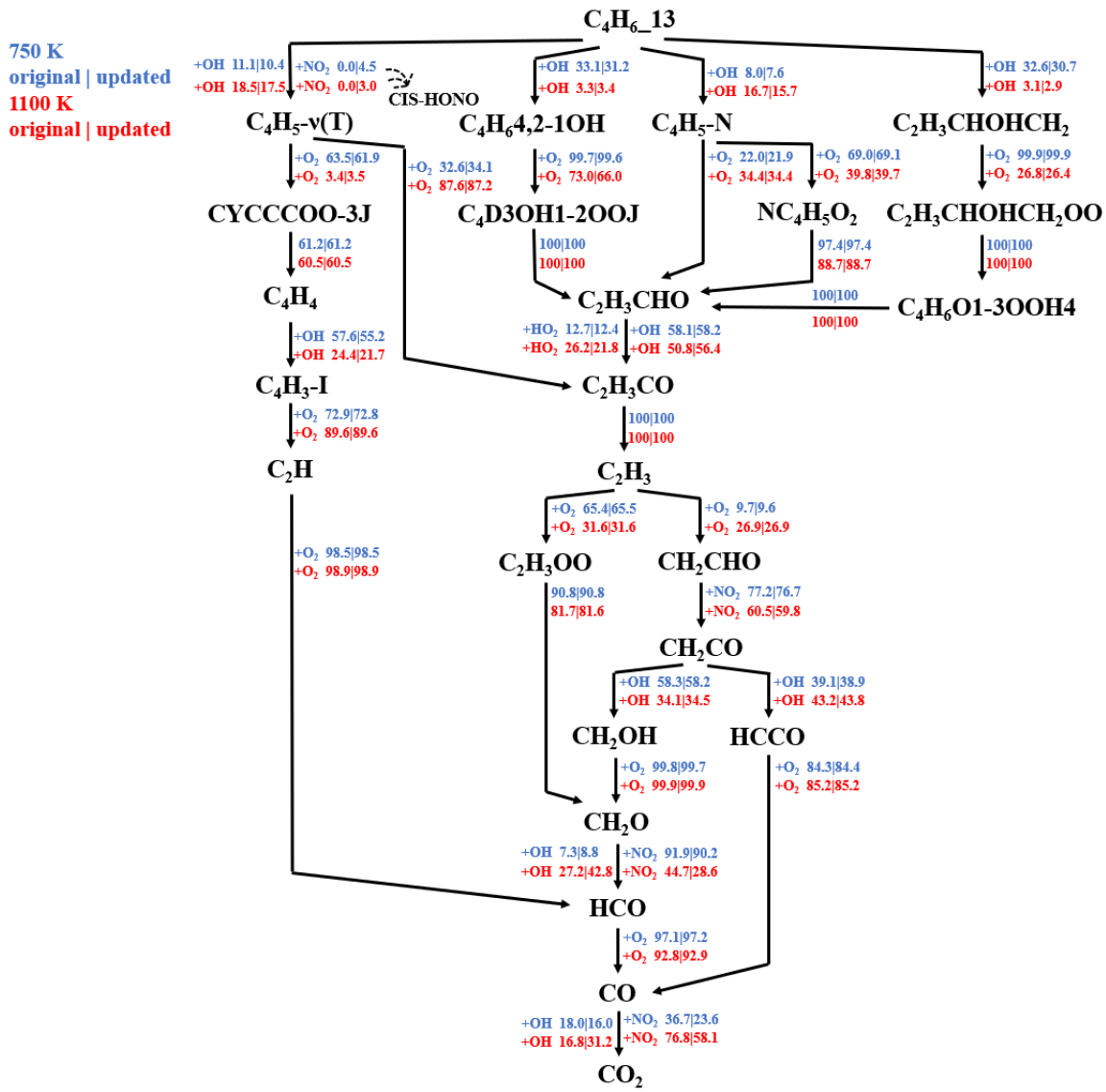

Figure 13. The flux analysis results for C_4H_6_13 ignition at P_C = 40 bar, T_C = 750 and 1100 K, equivalence ratio of 1, and with 1000 ppm NO_2 doped. Fluxes are computed at 1% C_4H_6_13 consumption.

4. Conclusions

This work presents a systematic study of H-atom abstractions by NO_2 from different sites of C_3–C_7 alkynes, dienes and triene to form different HNO_2 isomers (i.e., TRANS_HONO, HNO_2, and CIS_HONO). The geometry optimizations and vibrational frequencies of all the involved species are conducted at M06–2X/6–311++G(d,p) level of theory. The SPEs are determined at DLPNO-CCSD(T)/cc-pVDZ level of theory. The energy barriers of the investigated 24 reactions are obtained. The temperature dependent rate coefficients of these 24 reactions are proposed at the temperature range of 298.15–2000 K, based on conventional transition state theory with unsymmetric Eckart tunneling corrections. Updated rate constants for these reactions are further incorporated into a recently updated chemistry model, where their influences on model performance are investigated via comprehensive kinetic modeling. Sensitivity and flux analyses are further conducted to explore the chemical kinetics governing changes in model performances. The primary conclusions from this study are:

- Energy barriers at the primary (P), secondary (S), and tertiary (T) sites of alkynes, dienes, and triene decrease in the order of P > S > T. The C=C and C≡C functional groups considerably lower the energy barriers for abstracting the adjacent hydrogen atoms at the α carbon site, while H-atom abstractions at the C=C sites exhibit significantly higher energy barriers than all other sites. For all the species and reaction cites studied, the energy barriers for producing TRANS_HONO are consistently higher than those forming HNO_2 and CIS_HONO.
- After incorporating the rate parameters of the calculated reactions, the kinetic

model becomes considerably more reactive in predicting the autoignition of all alkynes and dienes, particularly for C_6H_{10}, with greater changes observed at low temperatures than at intermediate to high temperatures.

- Sensitivity and flux analyses reveal the kinetics governing the changes in model reactivity. With the updated rate parameters, there is an obvious increase and decrease in the contribution of H-atom abstractions by NO_2 and OH radicals, respectively, with the former and latter pathways being the top reactivity-promoting and reactivity-inhibiting reactions, which is mainly responsible for the increased model reactivity.
- This study highlights the critical role of H-atom abstractions from alkynes, dienes, and triene by NO_2, which have been missing from existing chemistry models. The obtained results emphasize the need for adequately representing these kinetics in new alkyne, diene, and triene chemistry models to be developed, by using the rate parameters determined in this study. There is also an urgent need for future experimental studies of fundamental combustion properties for NO_2-doped alkyne, diene, and triene mixtures.

Author Contributions

Zhengyan Guo: Methodology, Data curation, Formal analysis, Investigation, Software, Validation, Writing – original draft. **Hongqing Wu:** Methodology, Data curation, Formal analysis, Investigation, Software, Validation, Writing – original draft. **Ruoyue Tang:** Methodology, Data curation, Formal analysis, Investigation, Software, Validation, Writing – original draft. **Song Cheng:** Writing – original draft, Writing – review & editing, Supervision, Funding acquisition, Data curation, Conceptualization.

Xinrui Ren: Methodology, Software, Writing – review & editing. **Ting Zhang:** Methodology, Software, Writing – review & editing. **Mingrui Wang:** Methodology, Software, Writing – review & editing. **Guojie Liang:** Methodology, Software, Writing – review & editing. **Hengjie Guo:** Methodology, Software, Writing – review & editing.

Supporting Information

The supplementary material.docx contains T1 diagnostics, potential energy surface, comparison of rate coefficients, lowest-energy structure, and MESS input file.

Thermo.dat – the thermodynamics file in Chemkin format

Mech.inp – the chemical kinetics file in Chemkin format

Declaration of Competing Interests

The authors declare that they have no known competing financial interests or personal relationships that could have appeared to influence the work reported in this paper.

Acknowledgments

This material is based on work supported by the Research Grants Council of Hong Kong Special Administrative Region, China, under PolyU P0046985 for ECS project funded in 2023/24 Exercise and P0050998, and by the Natural Science Foundation of Guangdong Province under 2023A1515010976 and 2024A1515011486.

References

[1] Pan, J.; Tang, R.; Wang, Z.; Gao, J.; Xu, Q.; Shu, G.; Wei, H. An Experimental and Modeling Study on the Oxidation of Ammonia and N-Heptane with JSR. Proceedings of the Combustion Institute 2023, 39 (1), 477–485. https://doi.org/10.1016/j.proci.2022.07.193.

[2] Wei, H.; Zhu, T.; Shu, G.; Tan, L.; Wang, Y. Gasoline Engine Exhaust Gas Recirculation – A Review. Applied Energy 2012, 99, 534–544. https://doi.org/10.1016/j.apenergy.2012.05.011.

[3] Yao, M.; Zheng, Z.; Liu, H. Progress and Recent Trends in Homogeneous Charge Compression Ignition (HCCI) Engines. Progress in Energy and Combustion Science 2009, 35 (5), 398–437. https://doi.org/10.1016/j.pecs.2009.05.001.

[4] Cheng, S.; Saggese, C.; Goldsborough, S. S.; Wagnon, S. W.; Pitz, W. J. Chemical Kinetic Interactions of NO with a Multi-Component Gasoline Surrogate: Experiments and Modeling. Proceedings of the Combustion Institute 2023, 39 (1), 531–540. https://doi.org/10.1016/j.proci.2022.07.212.

[5] Hori, M.; Koshiishi, Y.; Matsunaga, N.; Glaude, P.; Marinov, N. Temperature Dependence of NO to NO2 Conversion by N-Butane and n-Pentane Oxidation. Proceedings of the Combustion Institute 2002, 29 (2), 2219–2226. https://doi.org/10.1016/S1540-7489(02)80270-X.

[6] Alzueta, M. U.; Hernández, J. M. Ethanol Oxidation and Its Interaction with Nitric Oxide. Energy Fuels 2002, 16 (1), 166–171. https://doi.org/10.1021/ef010153n.

[7] Abián, M.; Esarte, C.; Millera, Á.; Bilbao, R.; Alzueta, M. U. Oxidation of Acetylene−Ethanol Mixtures and Their Interaction with NO. Energy Fuels 2008, 22 (6), 3814–3823. https://doi.org/10.1021/ef800550k.

[8] Zhao, H.; Dana, A. G.; Zhang, Z.; Green, W. H.; Ju, Y. Experimental and Modeling Study of the Mutual Oxidation of N-Pentane and Nitrogen Dioxide at Low and High Temperatures in a Jet Stirred Reactor. Energy 2018, 165, 727–738. https://doi.org/10.1016/j.energy.2018.10.013.

[9] Marrodán, L.; Song, Y.; Lubrano Lavadera, M.; Herbinet, O.; de Joannon, M.; Ju, Y.; Alzueta, M. U.; Battin-Leclerc, F. Effects of Bath Gas and NOx Addition on N-Pentane Low-Temperature Oxidation in a Jet-Stirred Reactor. Energy Fuels 2019, 33 (6), 5655–5663. https://doi.org/10.1021/acs.energyfuels.9b00536.

[10] Menon, A. V.; Lee, S.-Y.; Linevsky, M. J.; Litzinger, T. A.; Santoro, R. J. Addition of NO2 to a Laminar Premixed Ethylene–Air Flame: Effect on Soot Formation. Proceedings of the Combustion Institute 2007, 31 (1), 593–601. https://doi.org/10.1016/j.proci.2006.08.105.

[11] Deng, F.; Zhang, Y.; Sun, W.; Huang, W.; Zhao, Q.; Qin, X.; Yang, F.; Huang, Z. Towards a Kinetic Understanding of the NOx Sensitization Effect on Unsaturation Hydrocarbons: A Case Study of Ethylene/Nitrogen Dioxide Mixtures. Proceedings of the Combustion Institute 2019, 37 (1), 719–726. https://doi.org/10.1016/j.proci.2018.07.115.

[12] Deng, F.; Huang, X.; Cheng, S.; Zhang, Y.; Huang, Z.; Tang, H.; Zheng, H.; Liu, X. Experimental and Modeling Study of NO2 Addition Effects on Autoignition Behavior of Propylene. Combustion and Flame 2024, 262, 113371. https://doi.org/10.1016/j.combustflame.2024.113371.

[13] Yuan, W.; Ruwe, L.; Schwarz, S.; Cao, C.; Yang, J.; Deutschmann, O.; Kohse-Höinghaus,

K.; Qi, F. Insights into the Interaction Kinetics between Propene and NOx at Moderate Temperatures with Experimental and Modeling Methods. Proceedings of the Combustion Institute 2021, 38 (1), 795–803. https://doi.org/10.1016/j.proci.2020.07.041.

[14] Cheng, S.; Saggese, C.; Goldsborough, S. S.; Wagnon, S. W.; Pitz, W. J. Unraveling the Role of EGR Olefins at Advanced Combustion Conditions in the Presence of Nitric Oxide: Ethylene, Propene and Isobutene. Combustion and Flame 2022, 245, 112344. https://doi.org/10.1016/j.combustflame.2022.112344.

[15] Chai, J.; Goldsmith, C. F. Rate Coefficients for Fuel + NO2: Predictive Kinetics for HONO and HNO2 Formation. Proceedings of the Combustion Institute 2017, 36 (1), 617–626. https://doi.org/10.1016/j.proci.2016.06.133.

[16] Wang, P.; Yan, J.; Yan, T.; Ao, C.; Zhang, L.; Lei, L. Kinetic Study of H-Abstraction and Preliminary Pyrolysis of n-Decane in Post-Injection Fuels. Combustion and Flame 2024, 262, 113367. https://doi.org/10.1016/j.combustflame.2024.113367.

[17] Wu, H.; Tang, R.; Ren, X.; Wang, M.; Liang, G.; Li, H.; Cheng, S. Understanding Key Interactions between NOx and C2-C5 Alkanes and Alkenes: The *Ab Initio* Kinetics and Influences of H-Atom Abstractions by NO2. Combustion and Flame 2025, 272, 113885. https://doi.org/10.1016/j.combustflame.2024.113885.

[18] Ohta, T.; Nagura, H.; Suzuki, S. Rate Constants for the Reactions of Conjugated Olefins with NO2 in the Gas Phase. International Journal of Chemical Kinetics 1986, 18 (1), 1–11. https://doi.org/10.1002/kin.550180102.

[19] Zhao, Y.; Truhlar, D. G. The M06 Suite of Density Functionals for Main Group Thermochemistry, Thermochemical Kinetics, Noncovalent Interactions, Excited States, and Transition Elements: Two New Functionals and Systematic Testing of Four M06-Class Functionals and 12 Other Functionals. Theor Chem Account 2008, 120 (1), 215–241. https://doi.org/10.1007/s00214-007-0310-x.

[20] McLean, A. D.; Chandler, G. S. Contracted Gaussian Basis Sets for Molecular Calculations. I. Second Row Atoms, Z=11–18. The Journal of Chemical Physics 1980, 72 (10), 5639–5648. https://doi.org/10.1063/1.438980.

[21] Hehre, W. J.; Ditchfield, R.; Pople, J. A. Self—Consistent Molecular Orbital Methods. XII. Further Extensions of Gaussian—Type Basis Sets for Use in Molecular Orbital Studies of Organic Molecules. The Journal of Chemical Physics 1972, 56 (5), 2257–2261. https://doi.org/10.1063/1.1677527.

[22] Andersson, M. P.; Uvdal, P. New Scale Factors for Harmonic Vibrational Frequencies Using the B3LYP Density Functional Method with the Triple-ζ Basis Set 6-311+G(d,p). J. Phys. Chem. A 2005, 109 (12), 2937–2941. https://doi.org/10.1021/jp045733a.

[23] Kendall, R. A.; Dunning, T. H., Jr.; Harrison, R. J. Electron Affinities of the First-row Atoms Revisited. Systematic Basis Sets and Wave Functions. The Journal of Chemical Physics 1992, 96 (9), 6796–6806. https://doi.org/10.1063/1.462569.

[24] Riplinger, C.; Neese, F. An Efficient and near Linear Scaling Pair Natural Orbital Based Local Coupled Cluster Method. The Journal of Chemical Physics 2013, 138 (3), 034106. https://doi.org/10.1063/1.4773581.

[25] Riplinger, C.; Sandhoefer, B.; Hansen, A.; Neese, F. Natural Triple Excitations in Local Coupled Cluster Calculations with Pair Natural Orbitals. The Journal of Chemical Physics 2013, 139 (13), 134101. https://doi.org/10.1063/1.4821834.

[26] Yang, C.; Chen, J.-T.; Zhu, X.; Bai, X.; Li, Y.; Yalamanchi, K. K.; Sarathy, S. M.; Scott Goldsborough, S.; Cheng, S.; Curran, H. J.; Zhou, C.-W. From Electronic Structure to Model Application of Key Reactions for Gasoline/Alcohol Combustion: Hydrogen-Atom Abstraction by CH3OȮ Radicals. Proceedings of the Combustion Institute 2023, 39 (1), 415–423. https://doi.org/10.1016/j.proci.2022.10.004.

[27] Zhang, P.; Klippenstein, S. J.; Law, C. K. Ab Initio Kinetics for the Decomposition of Hydroxybutyl and Butoxy Radicals of N-Butanol. J. Phys. Chem. A 2013, 117 (9), 1890–1906. https://doi.org/10.1021/jp400155z.

[28] Neese, F. ORCA 5.0.4, a quantum chemical program package; Max Planck Institute for Chemical Energy Conversion, Mülheim an der Ruhr, Germany, 2023. Available at: https://orcaforum.kofo.mpg.de.

[29] Georgievskii, Y.; Miller, J. A.; Burke, M. P.; Klippenstein, S. J. Reformulation and Solution of the Master Equation for Multiple-Well Chemical Reactions. J. Phys. Chem. A 2013, 117 (46), 12146–12154. https://doi.org/10.1021/jp4060704.

[30] Miller, J. A.; Klippenstein, S. J. Master Equation Methods in Gas Phase Chemical Kinetics. J. Phys. Chem. A 2006, 110 (36), 10528–10544. https://doi.org/10.1021/jp062693x.

[31] Georgievskii, Y.; Klippenstein, S. J. Strange Kinetics of the C2H6 + CN Reaction Explained. J. Phys. Chem. A 2007, 111 (19), 3802–3811. https://doi.org/10.1021/jp068430k.

[32] Eckart, C. The Penetration of a Potential Barrier by Electrons. Phys. Rev. 1930, 35 (11), 1303–1309. https://doi.org/10.1103/PhysRev.35.1303.

[33] Cheng, S.; Saggese, C.; Kang, D.; Goldsborough, S. S.; Wagnon, S. W.; Kukkadapu, G.; Zhang, K.; Mehl, M.; Pitz, W. J. Autoignition and Preliminary Heat Release of Gasoline Surrogates and Their Blends with Ethanol at Engine-Relevant Conditions: Experiments and Comprehensive Kinetic Modeling. Combustion and Flame 2021, 228, 57–77. https://doi.org/10.1016/j.combustflame.2021.01.033.

[34] Tang, R.; Han, Y.; Chen, H.; Qu, B.; Li, Y.; Lu, Z.; Xing, Z.; Cheng, S. Theoretical Study of H-Atom Abstraction by CH3OȮ Radicals from Aldehydes and Alcohols: Ab Initio and Comprehensive Kinetic Modeling. Combustion and Flame 2024, 259, 113175. https://doi.org/10.1016/j.combustflame.2023.113175.

[35] Ren, X.; Bai, X.; Jia, M.; Liu, S.; Han, Y.; Tang, R.; Cheng, S.; Zhou, C.-W.; Curran, H. J.; Li, Y. Ab Initio Kinetics for H-Atom Abstraction from C1–C5 Hydrocarbon and Oxygenated Species by CH3Ȯ Radicals. Combustion and Flame 2024, 263, 113410. https://doi.org/10.1016/j.combustflame.2024.113410.

[36] McNenly, M. J.; Whitesides, R. A.; Flowers, D. L. Faster Solvers for Large Kinetic Mechanisms Using Adaptive Preconditioners. Proceedings of the Combustion Institute 2015, 35 (1), 581–587. https://doi.org/10.1016/j.proci.2014.05.113.

[37] Mebel, A. M.; Diau, E. W. G.; Lin, M. C.; Morokuma, K. Theoretical Rate Constants for the NH3 + NOx → NH2 + HNOx (x = 1, 2) Reactions by Ab Initio MO/VTST Calculations. J. Phys. Chem. 1996, 100 (18), 7517–7525. https://doi.org/10.1021/jp953644f.

588 # List of Figures

589
590

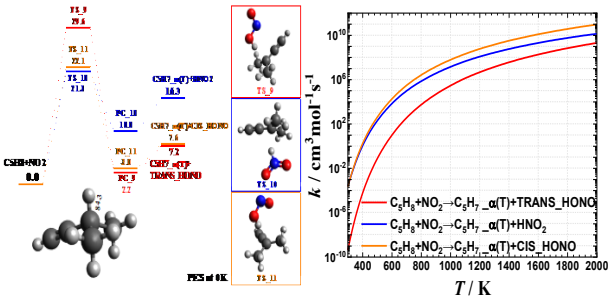
$C_5H_8+NO_2\rightarrow C_5H_7\_\alpha(T)+TRANS\_HONO$
$C_5H_8+NO_2\rightarrow C_5H_7\_\alpha(T)+HNO_2$
$C_5H_8+NO_2\rightarrow C_5H_7\_\alpha(T)+CIS\_HONO$
k / cm^{3}mol^{-1}s^{-1}
T / K

TOC graphic